JOURNAL OF AIRCRAFT
Vol. 43, No. 6, November–December 2006

Aerodynamic Design of Complex Configurations with Junctions

Salim Koc,* Hyoung-Jin Kim,† and Kazuhiro Nakahashi‡
Tohoku University, Sendai 980-8579, Japan

DOI: 10.2514/1.20723

An efficient aerodynamic design tool has been developed adopting a surface mesh movement method for body-installation junctions and an unstructured adjoint method. A three-dimensional unstructured Euler solver is used for flow analysis. Sensitivity analysis is conducted by a discrete adjoint solver. For the geometric modification around body-installation junctions, surface mesh points on aircraft components are moved directly on the curved body surface without any mapping or regeneration of the surface and volume mesh. The present design approach has been applied to ONERA M5 and DLR-F6 wing–body–nacelle–pylon configurations at transonic flow conditions. For ONERA M5, juncture between main wing and fuselage was redefined with wing geometry modification. For DLR-F6, juncture between wing and pylon was redefined with modification of both wing and pylon geometries. In both design examples, shock wave strength was remarkably reduced by the design process. The successful design results validate effectiveness and efficiency of the present design approach for complex configurations with junction interference effects.

I. Introduction

IN three-dimensional aerodynamic design optimization, complex geometries such as wing–body junction, integration of engine with pylon and nacelle, etc., still pose difficulties. For design modification of these body-installation junctions, junction lines need to be redefined, and surface and volume meshes should be regenerated or moved on both the wing and body.

For automated aerodynamic shape design of the junction region, overset-grid methods can be applied with relative ease [1,2]. Another approach is direct link of a design tool and a CAD system [3], which requires regeneration of surface and volume meshes. As an alternative way, Murayama et al. [4] developed a surface mesh movement method adopting a surface mapping method in which a three-dimensional surface mesh region to be moved is partially cut out to make a patch and mapped onto a two-dimensional parametric domain. Mesh points on the parameter domain are then moved appropriately and transformed back to the physical domain. For design problems the patch map and relating surface mesh should be regenerated in each design cycle. This may cause inefficiency for the whole design procedure.

Recently, Kim and Nakahashi [5] suggested a new surface mesh movement method for aerodynamic design of body-installation junctions. In the method, instead of mapping the surface mesh to a parametric patch mesh, surface mesh points move directly on curved body surface using spring analogy based on geodesic distance. New mesh locations are restricted to be on a smooth surface by a surface recovery method. Neither CAD-interface nor mesh regeneration is required. In this study, we apply the direct surface mesh movement method of [5] to aerodynamic design optimization of complex configurations with junctions.

Among several design optimization methods applicable to aerodynamic design problems, gradient-based methods have been used widely due to its well-developed numerical algorithms and relatively small computational burden. In the application of gradient-based methods to practical aerodynamic design problems, one of major concerns is accurate and efficient calculation of sensitivity gradient of aerodynamic objective function. During the last decade, the adjoint method has grown much attention as an efficient sensitivity analysis method for aerodynamic optimization because it allows calculation of sensitivity information independently of the number of design variables [6].

In this study, the surface mesh movement method is coupled with a gradient-based design optimization method. For the flow and sensitivity analysis, an unstructured finite volume Euler solver and its discrete adjoint code is utilized. The coupled design system is applied to design examples on complex configurations with junctions such as ONERA M5 and DLR F6 wing–body–nacelle–pylon configurations.

The remaining of this paper is composed as follows: In Sec. II, the direct surface mesh movement methodology for junction treatment is briefly explained. Design procedures including flow/adjoint analysis, optimization method, and sequence of design iteration are described in Sec. III. Design example on ONERA M5 is given in Sec. IV. Design of DLR-F6 with wing-nacelle–pylon interferences is conducted in Sec. V. Finally conclusions are made in Sec. VI.

II. Junction Treatment

In this section some brief information on the surface mesh movement method for junction treatment proposed in [5] is presented for completeness. More details on the surface mesh movement can be found in [5].

A. General Procedure

Figure 1 shows a schematic diagram for a wing-fuselage configuration in which both wing and fuselage geometry are modified. Solid and dotted lines represent initial modified geometries, respectively. For a wing-fuselage design problem as an instance, the procedure can be briefly described as follows:

1) Modify wing and fuselage geometry, respectively.

2) For the modified geometries, find new locations of the wing-fuselage junction nodes. Calculate geodesic distances from initial to new junction nodes along the faceted surface.

3) With the new body-fuselage junction node locations as boundary conditions, move wing surface mesh points along the faceted surface using a two-dimensional spring analogy based on the geodesic distances.

4) Conduct the same process as step 3 for fuselage surface mesh points.

Presented as Paper 4856 at the 17th AIAA Computational Fluid Dynamics Conference, Toronto Ontario, 6–9 June 2005; received 25 October 2005; revision received 21 March 2006; accepted for publication 20 April 2006.

*Graduate Student, Department of Aerospace Engineering; currently, Researcher, Toyota Motor Company, Toyota, Japan. Student Member AIAA.

†Research Associate, Department of Aerospace Engineering. Member AIAA.

‡Professor, Department of Aerospace Engineering. Associate Fellow AIAA.

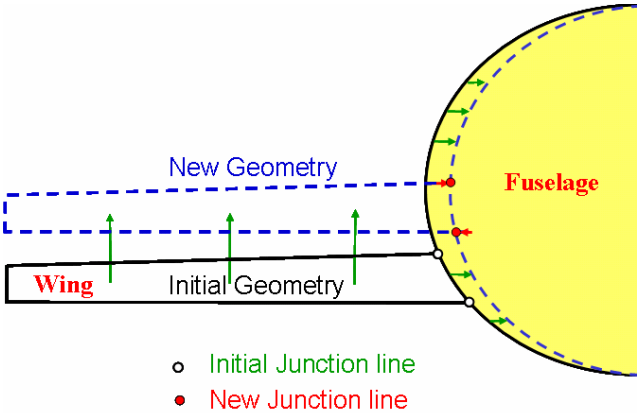

Fig. 1 Schematic diagram for geometry modification with wing–body juncture.

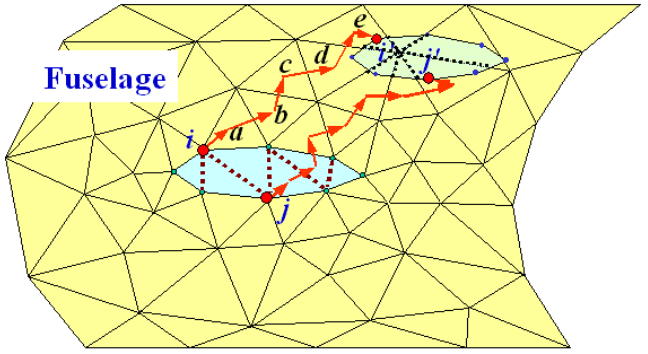

Fig. 2 Neighbor-to-neighbor search from initial to new junction location (Subsidiary cells are added by the edges in dotted lines).

5) Project new surface mesh points on the faceted surface to the smooth surface by a surface recovery method with the initial mesh as a background mesh.

6) Modify the volume mesh according to the new surface mesh.

B. Finding New Junction Location

To find a new position of juncture nodes, wing surface geometry needs to be extrapolated spanwisely when undefined wing geometry inside the fuselage is exposed by the geometric modification. For structured grids, spanwise mesh lines on a wing surface can be easily used for the extrapolation. On the other hand, unstructured meshes do not have such aligned mesh lines. Therefore at every junction nodes one need to calculate an extrapolating vector which is along local sweep angle and tangential to wing surface cell adjacent to the juncture. The next step is to find an intersection point where the extrapolation vector meets the fuselage surface, which is conducted using a neighbor-to-neighbor jump search method (see Fig. 2).

Although the neighbor-to-neighbor search enables an efficient one-dimensional search, it may fail to reach to the target point if there is a hole between the initial and target points. This is the case for the node j on the lower juncture line in Fig. 2. To circumvent this problem subsidiary surface cells are added in the junction hole as shown in dotted lines. The subsidiary cells are also helpful to recover fuselage geometry on the hole by a surface recovery method.

C. Surface Mesh Movement

When a new junction point is found by the neighbor-to-neighbor search method, one need to calculate the geodesic distance between the initial and new junction points which is used as boundary conditions for surface mesh movement. Geodesic distance is a distance between the points along curved surface. Euclidian distance is a good approximation to the geodesic distance only at regions of small curvature. Although Euclidian distance is much simpler to compute, the geodesic distance would give more robust results because the distance actually traveled by surface nodes is the geodesic distance which is always longer than Euclidian distance. If Euclidian distance is used for the surface mesh movement problem, one might obtain flipped surface meshes because of comparatively larger movement of junction nodes than inner surface nodes.

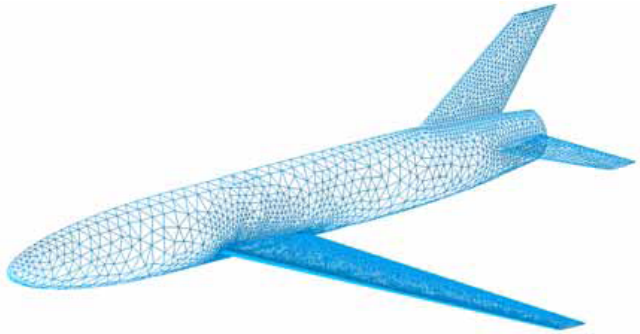

Fig. 3 Surface mesh for ONERA M5 wing–body configuration.

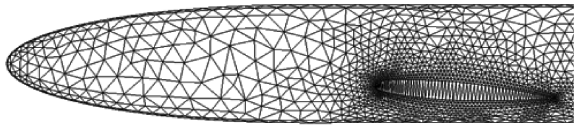

a) Fuselage surface mesh with subsidiary cells

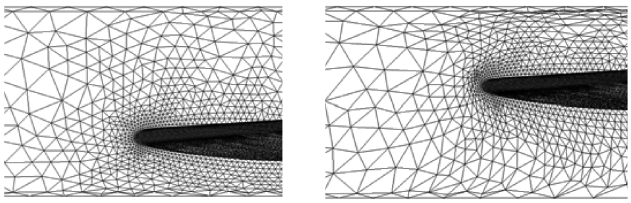

b) Vertical movement of ONERA M5 main wing: side view

Fig. 4 Sample movement of ONERA M5 main wing with the junction treatment method [5].

As a demonstration of the junction treatment, the method is applied to ONERA M5 configuration [5]. Figure 3 shows surface mesh of ONERA M5. Figure 4a represents the fuselage with surface mesh cells and additional cells on the junction hole. Figure 4b shows result of vertical movement of the main wing on the fuselage surface. Computational time for the surface mesh movement procedure is negligible compared with flow and sensitivity analysis in the design procedure.

III. Design System

The junction treatment method described in Sec. II is coupled with existing aerodynamic design optimization tool [7,8] composed of an unstructured flow solver, a discrete adjoint code, gradient-based optimizers, surface mesh perturbation, and volume mesh modification routines.

A. Flow and Sensitivity Analysis

A three-dimensional unstructured Euler solver [9] is used for flow analysis. The governing Euler equations are solved by a finite volume cell-vertex scheme. The control volumes are nonoverlapping dual cells constructed around each cell node. Each edge connecting two nodes is associated with vector area of control surface, and gas dynamic fluxes are computed through the areas. Primitive gas dynamic variables are linearly reconstructed inside the median-dual

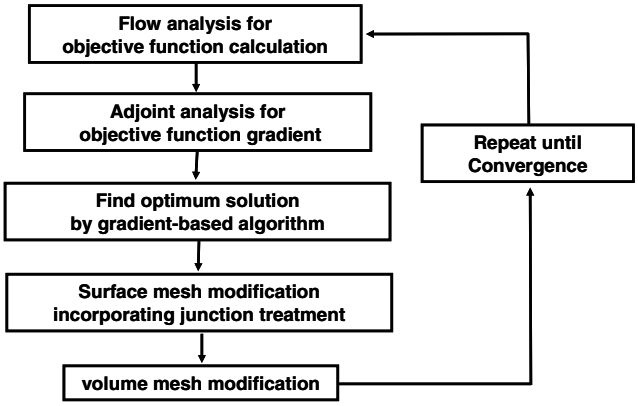

Fig. 5 Flow chart of the design procedure.

control volume for second order spatial accuracy and multiplied by a limiter function for monotonicity preservation. After the reconstruction, a flux quadrature is performed around each control volume using a single point along each face of the control volume. The flux is computed by an approximate Riemann solver. For the time integration, the lower-upper symmetric Gauss Seidel (LU-SGS) implicit method is adopted [10].

For efficient calculation of sensitivity information, a discrete adjoint solver developed from the flow solver described above is used [7]. The discrete adjoint solver utilizes the same time integration method as the flow solver. By the use of the adjoint method, computational cost for sensitivity analysis is independent of the number of design variables.

B. Optimization Algorithms

In this study, we adopt gradient-based optimization methods utilizing gradient information of objective function provided by the adjoint solver. Selection of specific optimization method depends on the selection of design variables. When all the surface mesh points are adopted as design variables, the traction method coupled with the steepest descent method is used with linear or quadratic line search [8]. If shape functions are employed for geometry perturbation, we use the sequential quadratic programming (SQP) method [11] in which the objective function is approximated by a quadratic Taylor series expansion to create a direction-finding problem. Detailed algorithms and methodologies of the SQP method are described in [11].

C. Design Procedure

Figure 5 shows the general design procedure in this study. With an objective function and its gradient information computed by flow and adjoint analysis, respectively, an optimizer finds a new set of design variables for a local optimum solution along the search direction. A new surface geometry is then constructed following the design variables. If juncture regions are modified by the design, the juncture treatment procedure described in Sec. II is applied to get a new surface geometry with neither CAD intervention nor time-consuming remeshing process of surface and volume meshes during the design cycle. After the surface mesh modification, volume mesh is also modified accordingly. In this study, volume mesh is modified by a robust volume mesh modification method based on a torsion spring analogy proposed by Murayama et al. [4]. With the newly modified meshes, flow analysis is conducted to calculate the objective function of the design problem. Then adjoint analysis is conducted if necessary. This design iteration is repeated within user-specified maximum iteration number until reduction amount of the objective function becomes negligible.

IV. Design Example 1: ONERA M5 Configuration

A. Definition of Design Problem

The first design example is ONERA M5 configuration in a transonic regime. The surface mesh is generated by the direct advancing front method coupled with the geometrical feature extraction on the STL (stereolithography) data format [12]. The tetrahedral volume mesh is generated by a Delaunay-type generation method [13]. The computational grid of ONERA M5 contains 113,132 mesh points and 606,110 tetrahedral. Design conditions are free stream Mach number M_∞ of 0.84 and lift coefficient C_L of 0.256 with initial angle of attack $\alpha = -1.0$ deg.

Design problem is defined as follows:

$$\begin{aligned} &\text{Minimize } C_D \\ &\text{Subject to } C_L \geq C_L^* \\ &\qquad\qquad V \geq \text{initial } V \end{aligned}$$

where C_D and C_L are drag and lift coefficients, respectively. V is wing volume, and C_L^* is initial lift coefficient.

If the lift constraint is dealt as an explicit constraint in the optimization procedure, it requires an additional adjoint analysis for the calculation of gradient of C_L per each design cycle. In this study, therefore, the lift constraint is satisfied running the flow solver in a fixed-lift mode, in which angle of attack is adjusted on the fly based on $C_{L\alpha}$. The objective function is modified considering the lift constraint as follows [9].

$$F = C_D - \frac{C_{D_\alpha}}{C_{L_\alpha}}(C_L - C_L^*) \tag{1}$$

where the second term in the right-hand side containing lift coefficients acts as a penalty term which prevents the design from reducing the drag by simply reducing the lift. The volume constraint is imposed by a gradient projection method [8].

B. Surface Geometry Modification

In this example, geometry modification is made by the mesh point method which uses surface mesh points as design variables. For a smooth variation of the geometry, we employ the concept of the traction method combined with spring analogy [8]. Surface mesh points and edges are modeled as bending and tension springs, respectively. Negative gradient of objective function is imposed on the surface mesh points as external forces, and deformation of the surface spring system is calculated. Along the resultant variation of the geometry, a line search is conducted to find the optimum solution. Details of the traction method can be found in Kim et al. [8]. In the present case, all the surface mesh points on the main wing including wing-fuselage junction points are selected as design variables and allowed to move in the vertical direction only.

All the computations in this study are conducted on NEC SX-7 vector supercomputer located at Information Synergy Center of Tohoku University.

C. Design Results

Table 1 summarizes design results for ONERA M5. The drag coefficient was reduced by 19 counts while satisfying the lift coefficient and almost satisfying the wing volume constraint. Figure 6 shows the convergence history of the design process. Strength of the λ shock wave is remarkably reduced by the design as shown in Fig. 7 especially near the wing–body junction. Figure 8 shows wing section

Table 1 ONERA M5 design results at $M_\infty = 0.84$ and $C_L = 0.256$

	C_L	C_D	Wing volume
Initial	0.2560	0.0266	5.00×10^{-4}
Design	0.2561	0.0248	4.93×10^{-4}
Δ(%)	0.04	−6.98	−1.40

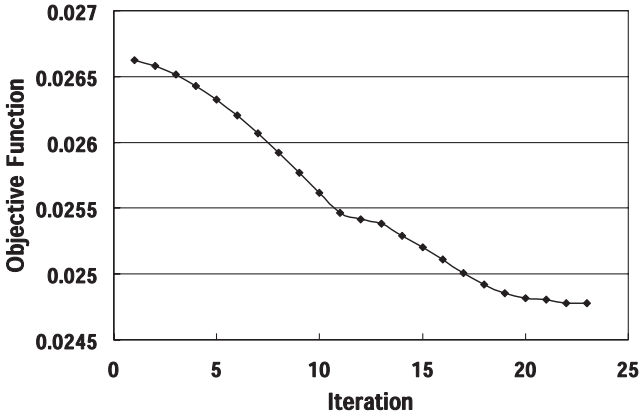

Fig. 6 ONERA M5 design history.

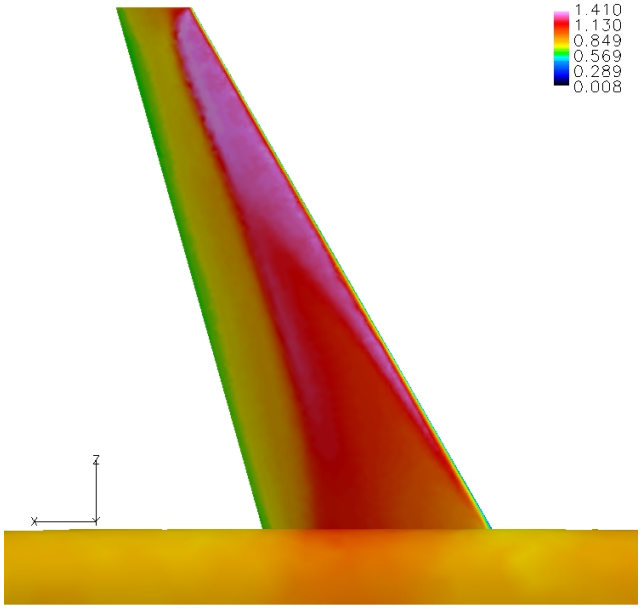

a) Initial

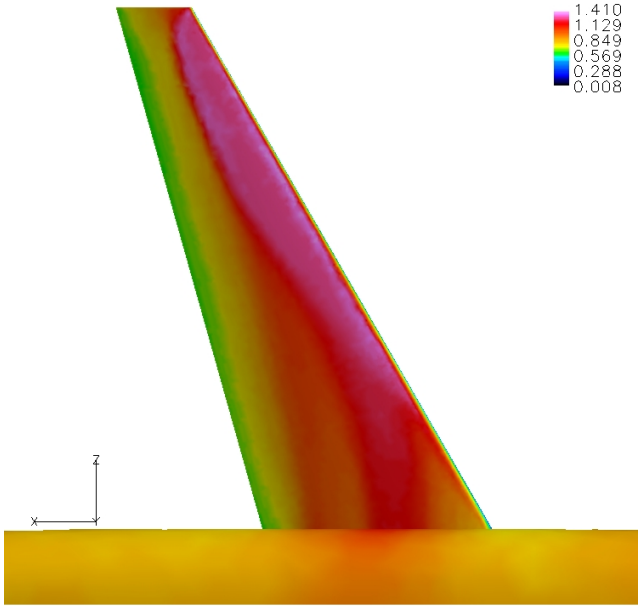

b) Design

Fig. 7 Mach contours of ONERA-M5 wing upper surface ($M_\infty = 0.84$ and $C_L = 0.256$).

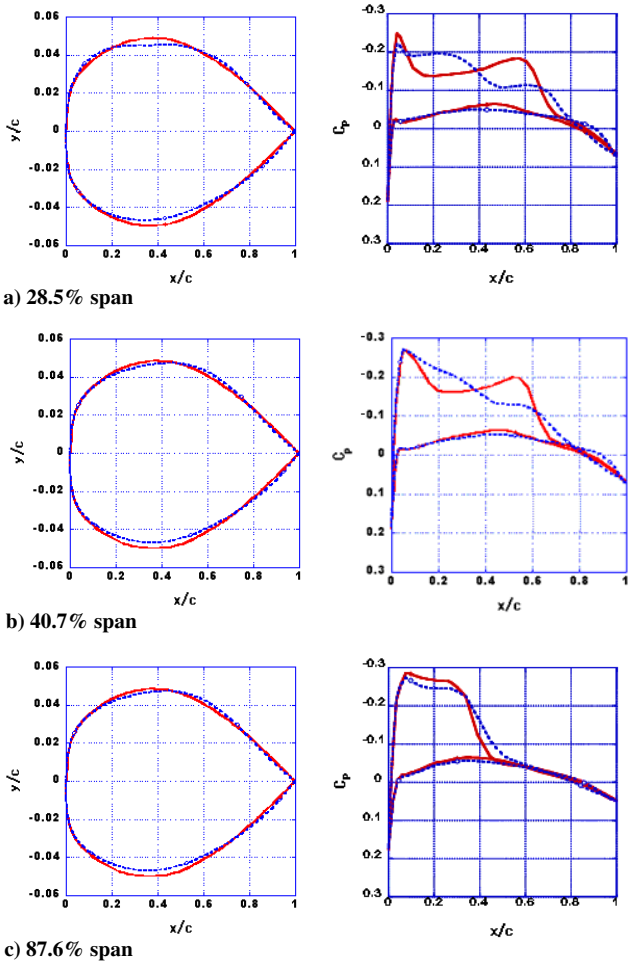

a) 28.5% span

b) 40.7% span

c) 87.6% span

Fig. 8 Section shapes and surface pressure distributions for the ONERA M5 design case at $M_\infty = 0.84$ and $C_L = 0.256$ (solid lines: initial; dotted lines: design).

shapes and surface pressure distributions, from which reduction of shock strength and smooth geometric variations can be noted.

V. Design Example 2: DLR-F6 wing–body–nacelle–pylon Configuration

A. Definition of Design Problem

Installation of nacelle, pylon, and engine components has significant effects on aircraft performances especially at high speed flows. There have been several experiments and theoretical investigations on thee aerodynamic interference effects [14]. The present design methodology can be a powerful tool for aerodynamic design of complex aircraft configurations with junction interference effects. As a design example of aircraft configuration with wing-nacelle–pylon interference, here we apply the present method to DLR-F6 wing–body–nacelle–pylon configuration.

Computational mesh for the configuration is shown in Fig. 9 containing 463,846 nodes and 2,565,463 tetrahedral. Design conditions are freestream Mach number of 0.74 and C_L of 0.14 with initial angle of attack $\alpha = -2.9$ deg, which corresponds to a climb condition for transonic transports.

At the flow condition, flow over initial pylon surface is highly accelerated because of the interference of wing, nacelle, and pylon. The pylon surface Mach number reaches up to 1.72 leading to a strong shock wave (See Fig. 10), which may cause a buffet. Buffet is a shock-boundary layer interaction phenomenon causing shock wave oscillation and subsequent oscillation of lift and pitching moment. In transonic regime, buffet is a major limiting factor for the cruise speed and lift. Objective of this design example is to minimize

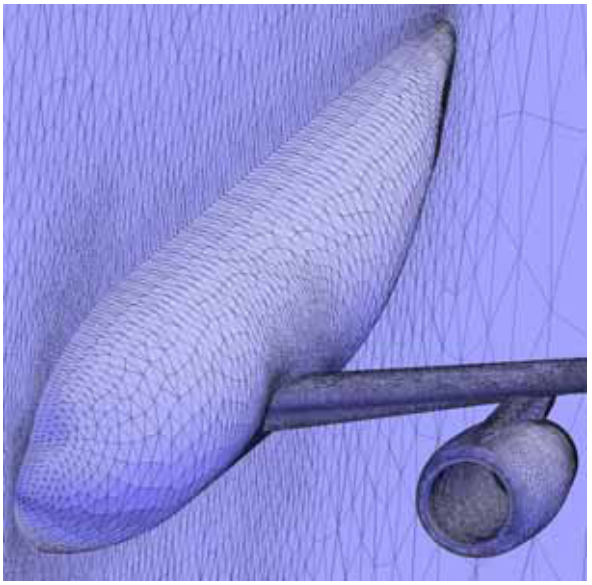

Fig. 9 Computational mesh for DLR-F6 configuration.

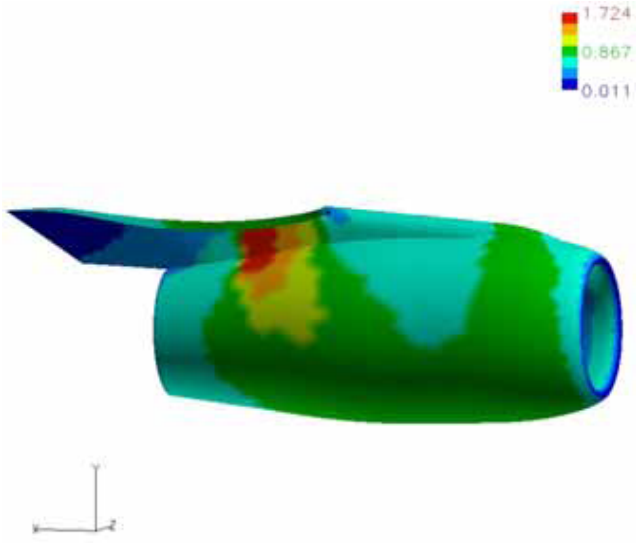

Fig. 10 Mach contours on DLR-F6 nacelle–pylon surface.

drag and eliminate the strong shock wave on the pylon to reduce buffet risk at the design condition.

Design constraints are imposed as follows:

1) No buffet on the pylon surface.

2) $C_L \geq C_L^*$ (Initial C_L).

3) Wing section maximum thickness $\geq$ initial wing section maximum thickness (@34% chord).

4) Pylon section maximum thickness $\geq$ initial pylon section maximum thickness (@25% chord).

The constraint of buffet suppression is implemented by imposing upper bound of surface Mach numbers as 1.25 on the pylon. This constraint is treated as a penalty term added to the objective function F as follows:

$$F = C_D + w \sum_{\text{surface}} \max(0, p_{\text{lim}} - p_{\text{surf}}) \Delta S \qquad (2)$$

where w is a weighting factor multiplied to the penalty term, and p_{lim} is pressure limit calculated from the Mach number of 1.25 by the isentropic relation, p_{surf} is pressures on pylon surface, and ΔS is area of a surface cell. Local pressure values are constrained instead of local Mach numbers for simplicity in differentiation of the objective function with respect to primitive flow variables for adjoint formulation [15].

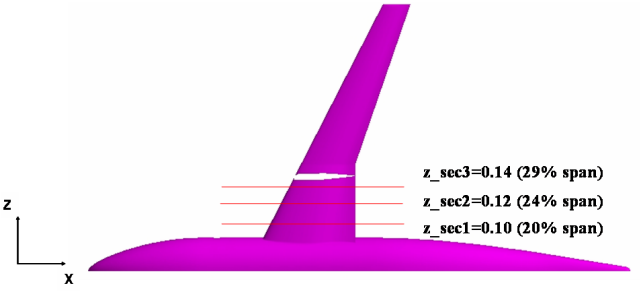

a) Inboard wing design sections

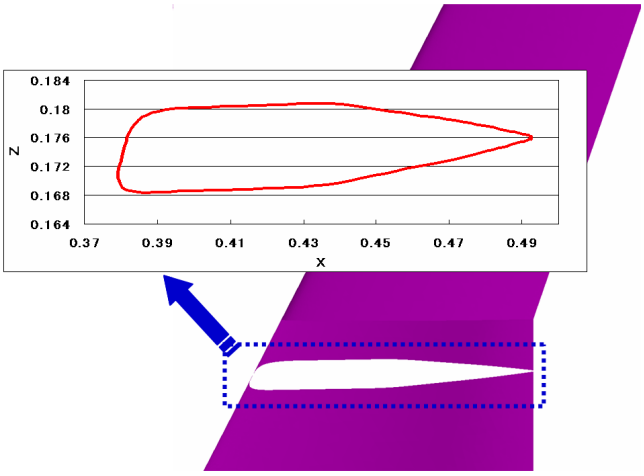

b) Pylon design section (Wing-pylon junction)

Fig. 11 Design sections for DLR-F6.

The lift constraint is satisfied by running the flow solver in the fixed-lift mode as was in the previous design example shown in Eq. (1). Geometric constraints such as wing and pylon section thickness constraints are explicitly treated in the SQP optimizer.

B. Surface Geometry Modification

Geometry modifications are made by inboard wing section shape deformation, pylon section shape deformation, nacelle vertical movement, and nacelle pitch angle variation. As shown in Fig. 11a, we use three design sections along the inboard wingspan. Wing–pylon junction is also used as a design section for pylon geometry perturbation (see Fig. 11b). The inboard wing and pylon section geometries are modified by adding a linear combination of Hicks–Henne shape functions [16]. On each of the four design sections 20 design variables are defined for Hicks–Henne shape functions. With the new geometry at the design sections, node points on the inboard wing surface and pylon surface are linearly interpolated independently. Then the surface mesh movement approach presented in Kim and Nakahashi [5] and also described in Sec. II is applied to the wing–pylon juncture. In addition to the 80 design variables for the design sections vertical movement and pitch angle variation of nacelle are also considered as design variables. Thus the number of design variables is 82 in all.

Regarding the nacelle movements, pylon geometry is deformed accordingly with fixed nacelle–pylon and wing–pylon junctions.

Table 2 DLR F6 design results at $M_\infty = 0.74$ and $C_L = 0.14$

	C_L	C_D
Initial	0.1402	0.0080
Design	0.1401	0.0064
Δ(%)	−0.02	−19.7

Pylon deformation can be conducted by a simple spring analogy with spring constant based on edge length. Boundary conditions for the pylon deformation are imposed as follows: displacement of pylon-wing junction points as zero, displacement of pylon-nacelle junction points as the nacelle displacement, and pylon leading and trailing edges are linearly interpolated from the lower and upper boundaries based on the x coordinate.

C. Design Results

Table 2 summarizes results of DLR-F6 design. By the design process, drag coefficient was reduced by 16 counts from the initial value. The maximum Mach number of 1.72 on the pylon surface of initial geometry was reduced to 1.27 by the design, which almost satisfies the Mach number constraint. Further, the maximum thicknesses of the wing sections and pylon section are maintained during the design process, although not shown in numbers here. It can be noted in Fig. 12 that the strength of shock wave on the wing lower surface and pylon surface is remarkably reduced through the design procedure. The nacelle has moved upward and pitched up by the design process (see Fig. 12b).

Figures 13 compare section shapes and pressure distributions at wing design sections. Section pressure distributions show that the shock wave on the lower surface has been almost removed. Further, it can be noted that maximum thicknesses of initial wing sections are maintained during the design process. The most remarkable section shape variation was made at 29% wingspan (Fig. 13c) which is the nearest design section to the pylon. The wing lower surface near leading edge at 29% span has become flat compared with the initial section shape. This shape change seems to be related with the shape of "channel-like flow path" surrounded by wing, nacelle, and pylon.

A change of pylon section shape at wing–pylon junction and surface pressure distributions are presented in Fig. 14, which also shows shock removal by the design.

Figure 15 shows Mach contours at 34% span location, which is very close to the pylon surface and gives the flow information at inboard wing–pylon-nacelle region. As can be seen in Fig. 14a, a channel-like flow path is formed between wing, nacelle, and pylon surfaces of initial geometry. Entering the channel, the flow is accelerated and reaches to a supersonic region at downstream of throat. The supersonic region is then terminated by a strong normal shock wave. On the other hand, in Fig. 14b, the supersonic channel flow of the design configuration is slightly accelerated, which is then compressed almost isentropically without a shock wave. The initial geometry has a flow path of "congergent–divergent nozzle" shape, whereas the channel shape has been straightened by the design.

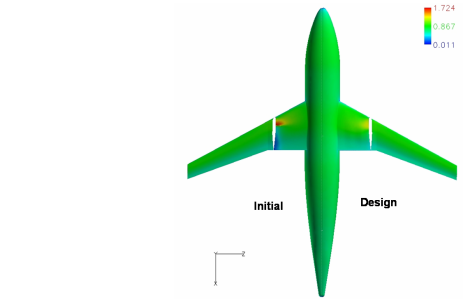

a) Wing-Body lower surface

b) Wing-Body-Nacelle-Pylon surface

Fig. 12 DLR-F6 design results: surface Mach contours ($M_\infty = 0.74$, $C_L = 0.140$).

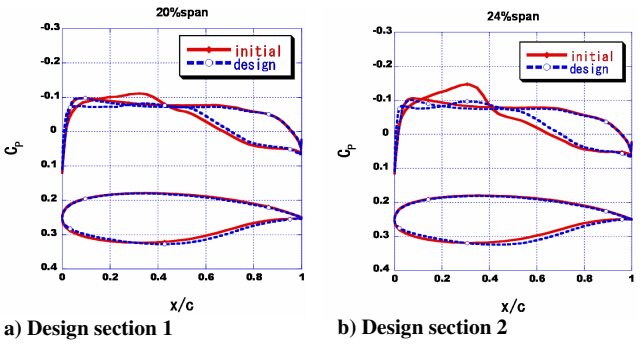

a) Design section 1

b) Design section 2

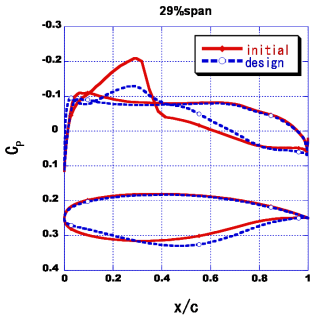

c) Design section 3

Fig. 13 Wing section shapes and pressure distributions of the DLR-F6 design case. ($M_\infty = 0.74$, $C_L = 0.140$).

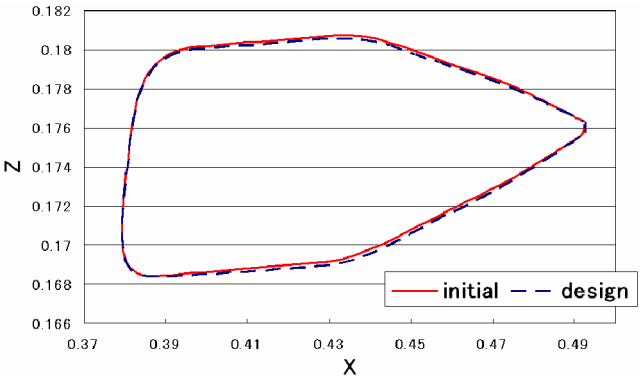

a) Pylon section shape

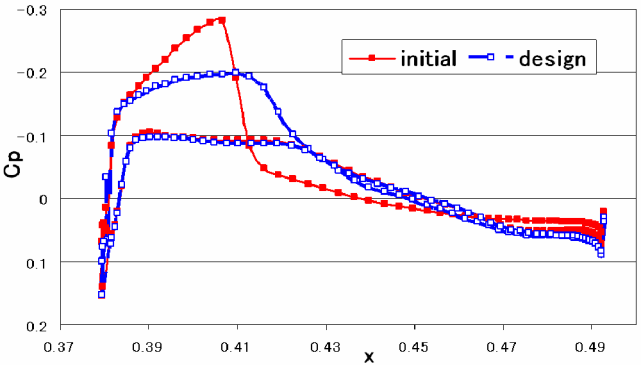

b) Surface pressure distribution

Fig. 14 DLR-F6 design results: pylon section shapes and pressure distributions at wing–pylon junction.

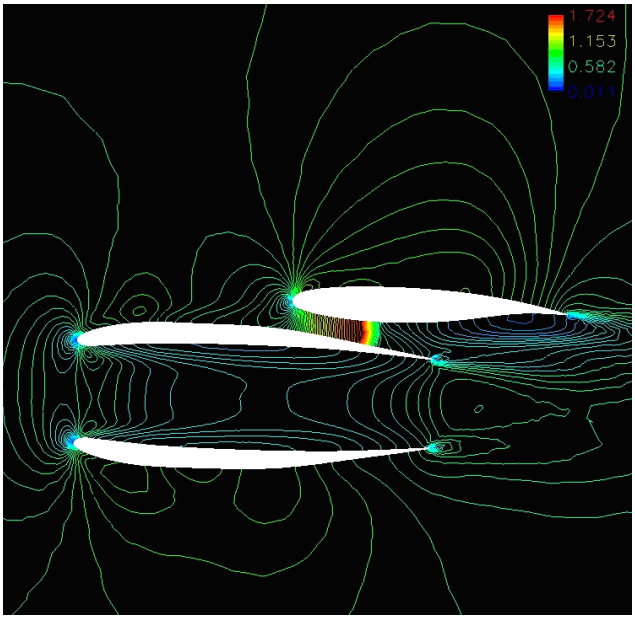

a) Initial

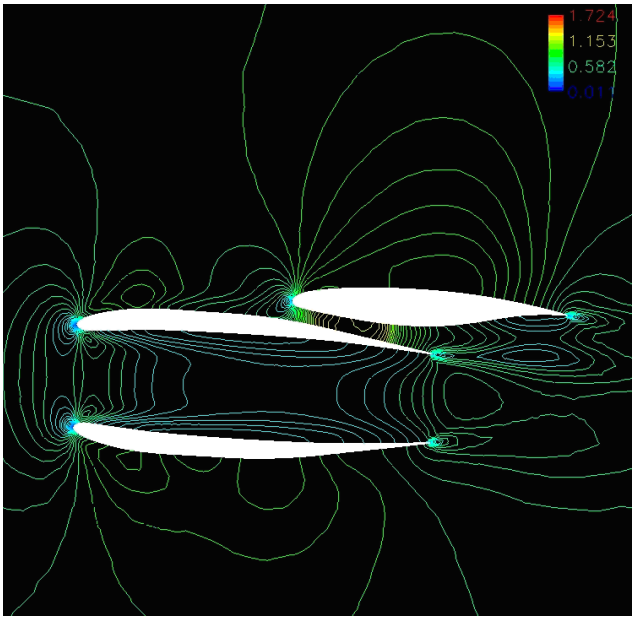

b) Design

Fig. 15 DLR-F6 design results: Mach contours at 34% wingspan.

The present design results for DLR-F6 configuration with flat lower wing surface near leading edge and nacelle moved-upward and piched-up may have negative effects on its cruise performance. To cope with this problem, multipoint design needs to be conducted for both cruise and climb conditions.

VI. Conclusions

An efficient aerodynamic design tool has been developed for complex geometries with junctions. For the flow and sensitivity analysis, an unstructured Euler solver and its discrete adjoint code was utilized. For the geometric modification around body-installation junctions, surface mesh points on aircraft components are moved directly on the curved body surface without any mapping or regeneration of the surface and volume mesh. Design examples were demonstrated for ONERA M5 and DLR-F6 wing–body–nacelle–pylon configurations. For ONERA M5, the junction between the main wing and fuselage was redefined for wing geometry modification. For DLR-F6, the junction between the wing and pylon was redefined for the modification of both wing and pylon geometry. Successful design results verify effectiveness of the present approach for design of aircraft configurations with junction interferences.

References

[1] Steger, J. L., Dougherty, F. C., and Benek, J. A., "A Chimera Grid Scheme (Multiple Overset Body-Conforming Mesh System for Finite Difference Adaptation to Complex Aircraft Configurations)," *Advances in Grid Generation; Proceedings of the Applied Mechanics, Bioengineering, and Fluids Engineering Conference*, 1983, pp. 59–69.

[2] Nakahashi, K., Togashi, F., and Sharov, D., "Intergrid-Boundary Definition Method for Overset Unstructured Grid Approach," *AIAA Journal*, Vol. 38, No. 11, 2000, pp. 2077–2084.

[3] Jameson, A., Martinelli, L., and Haimes, B., "Aerodynamic Shape Optimization of Complete Aircraft Configurations Using Unstructured Grids," AIAA 2004-0533, January 2004.

[4] Murayama, M., Nakahashi, K., and Matsushima, K., "A Robust Method for Unstructured Volume/Surface Mesh Movement,," *Transactions of the Japan Society for Aeronautical and Space Sciences*, Vol. 46, No. 152, August 2002, pp. 104–112.

[5] Kim, H. J., and Nakahashi, K., "Surface Mesh Movement for Geometric Modification of Body-Installation Junctions," *Proceedings of the Third International Conference on Computational Fluid Dynamics (ICCFD3)*, 2004.

[6] Jameson, A., "Aerodynamic Shape Optimization Using the Adjoint Method," *Lecture Series at the Von Karman Institute for Fluid Dynamics*, von Karman Institute, Brussels, Belgium, 2003.

[7] Kim, H. J., Sasaki, D., Obayashi, S., and Nakahashi, K., "Aerodynamic Optimization of Supersonic Transport Wing Using Unstructured Adjoint Method," *AIAA Journal*, Vol. 39, No. 6, June 2001, pp. 1011–1020.

[8] Kim, H. J., Koc, S., and Nakahashi, K., "Surface Modification Method for Aerodynamic Design Optimization," *AIAA Journal*, Vol. 43, No. 4, April 2005, pp. 727–740.

[9] Nakahashi, K., Ito, Y., and Togashi, F., "Some Challenges of Realistic Flow Simulations by Unstructured Grid CFD," *International Journal for Numerical Methods in Fluids*, Vol. 43, No. 6–7, November 2003, pp. 769–783.

[10] Sharov, D., and Nakahashi, K., "Reordering of Hybrid Unstructured Grids for Lower-Upper Symmetric Gauss-Seidel Computations," *AIAA Journal*, Vol. 36, No. 3, 1998, pp. 484–486.

[11] Vanderplaats, G. N., *Numerical Optimization Techniques for Engineering Design: with Applications*, McGraw–Hill, New York, 1984, pp. 195–199.

[12] Ito, Y., and Nakahashi, K., "Direct Surface Triangulation Using Stereolithography Data," *AIAA Journal*, Vol. 40, No. 3, 2002, pp. 490–496.

[13] Sharov, D., and Nakahashi, K., "A Boundary Recovery Algorithm for Delaunay Tetrahedral Meshing," *Proceedings of the 5th International Conference on Numerical Grid Generation in Computational Field Simulations*, Mississipi State University, MS, 1996, pp. 229–238.

[14] Rossow, C. C., Godard, J. L., Hoheisel, H., and Schmitt, V., "Investigations of Propulsion Integration Interference Effects on a Transport Aircraft Configuration," *Journal of Aircraft*, Vol. 31, No 5, 1994, pp. 1022–1030.

[15] Kim, H. J., Obayashi, S., and Nakahashi, K., "Flap-Deflection Optimization for Transonic Cruise Performance Improvement of Supersonic Transport Wing," *Journal of Aircraft*, Vol. 38, No. 4, 2001, pp. 709–717.

[16] Hicks, R. M., and Henne, P. A., "Wing Design by Numerical Optimization," *Journal of Aircraft*, Vol. 15, No. 7, 1978, pp. 407–412.